Shear localization in dynamic deformation of copper single crystals

S. X. LI*, R. Q. YANG, J. W. LI and Z. F. ZHANG

Shenyang National Laboratory for Materials Science, Institute of Metal Research,
The Chinese Academy of Sciences, Shenyang, 110016, China

Dynamic deformation of copper single crystals, especially of fatigued copper single crystals with different orientations, was conducted on a split-Hopkinson pressure bar apparatus. The strain rates were in the range $2 - 9 \times 10^3 \, s^{-1}$. After dynamic deformation, the adiabatic shear bands (ASBs) were examined in a light microscope and SEM. The width and spacing of ASBs formed under different strain rates in a fatigued copper single crystal were measured and the spacing of ASBs is one-order of magnitude smaller than the theoretical predictions. The possible reasons for the discrepancy were discussed. The critical strains for the ASB formation in four different orientated single crystals at stain rate of about $4 \times 10^3 \, s^{-1}$ were determined by examining the post-deformation specimens and dynamic stress–strain curves. It is clearly indicated that the critical strains for the ASB formation are orientation-dependent in copper single crystals. A simple microscopic mechanism for ASB formation in fatigued single crystals was proposed.

1. Introduction

Shear localization has been found to be an important and sometimes dominant deformation and fracture mode in metals. As a model material, the deformation behaviours and the dislocation structures of copper single crystals have been well studied under different loading conditions.

There are several kinds of bands appearing in the copper single crystals under monotonic, cyclic or dynamic loadings. During monotonic loading, the slip bands (sometimes called slip lines) appear on the sample surface, however, no characteristic dislocation configurations underneath correspond to these slip bands. During cyclic deformation, among many slip bands, the persistent slip bands (PSBs) appear and a corresponding characteristic dislocation pattern called the ladder structure could be found in the samples. The formation of PSBs in copper single crystals has been widely studied since 1950s [1–5]. The dislocation structures of PSBs are well understood nowadays [6–8]. The investigation on nucleation, growth and, sometimes, annihilation of the characteristic dislocation arrangements of PSBs has been the subject of recent experimental work [9–18]. Under consecutive cyclic loading,

---

*Corresponding author. Email: shxli@imr.ac.cn

the deformation bands (DBs) occur finally in the copper single crystals [19, 20]. There are mainly two types of DBs, i.e. DBI and DBII that are parallel and perpendicular to the primary slip plane, respectively. The width of these bands (20–40 μm) is usually much larger than that of PSBs (1–2 μm). The formation mechanism of DBs was discussed by Li *et al.* [20].

Highly localized deformation, generally referred to as adiabatic shear bands (ASBs), can occur in a variety of metals when deformed at high strain rates, such as high-speed machining, ballistic impact, high-velocity punching and metal forming. Zener and Hollomon [21] were probably the first to recognize that rapid plastic working, accompanied by self-heating and subsequent strain-softening, was an agent that could lead to material instability, which manifested itself as narrow regions of intense shear. Theoretical work was also developed along with the experimental progress [22–24]. To explore the initiation and growth mechanisms of ASBs, the observation of microstructure evolution within the bands is valuable in examining the post-deformation specimens [25, 26].

Dynamic shear localization is also observed on the scale of single crystals [27, 28]. However, systemic investigation on dynamic deformation of single crystals with different orientations is still rare. Currently, the investigation on ASB formation is concentrated on polycrystals. Since the widths of ASBs usually range from 1 to 100 μm, which covers the grain sizes (5–50 μm) of most conventional metals and alloys. If the width of an ASB is smaller than the grain size, the ASB may pass through the grain interior; therefore, investigation on ASB formation in single crystals is necessary. On the other hand, even if the width of an ASB is larger than the grain size, the initiation of the ASB may still start from a grain boundary or other imperfections within the grain, the initial width may still be smaller than the grain size, only during dynamic deformation process, and the width of an ASB grows to a certain size. In this case, investigation on ASB formation at the initial stage in single crystals is still desired.

As mentioned above, the self-heating caused by rapid plastic deformation and subsequent strain-softening was a key factor to lead to material instability. However, the geometric softening caused by crystallographic rotation might also play an important role in the instability for single crystals during dynamic deformation. In this sense, the single crystals with different orientations are essential for investigating the mechanism of ASB formation.

Two cases of shear band formation were analyzed. The ASB formation under high strain rate was modelled by continuum mechanics, in which the thermal softening was considered and the geometric softening was neglected, for example [22–24]. By contrast, the shear band formation under conventional rolling process was modelled by meso-mechanics, in which the geometric softening was considered and the thermal softening was neglected, for example [29]. In fact, the thermal softening, geometric softening, as well as the damage softening [30] are all potential factors for ASB formation. However, to the authors' knowledge no available experimental data indicates that geometric softening is one of the key factors for ASB formation.

Recently, the electron channelling contrast (ECC) technique has received much attention for studying dislocation configurations in deformed materials [17–19, 31–33]. In this paper, the ASB microstructures are observed by the ECC technique.

The ASB spacing and width, the critical strains for ASB formation and orientations of ASB planes are reported in detail.

2. Experimental

Copper single crystals of 99.999% purity with loading axis parallel to $[\bar{1}\ 2\ 4]$, $[\bar{3}\ 4\ 7]$, $[\bar{4}\ 15\ 16]$ and $[\bar{1}\ 8\ 11]$ orientations were grown by the Bridgman method. Three groups of experiments were conducted.

(1) Specimens without pre-deformation before dynamic loading; the dimensions of the specimens are $5 \times 5 \times 8$, $5 \times 5 \times 4$ and $5 \times 5 \times 2\,\text{mm}^3$.

(2) Specimens had undergone cyclic deformation before dynamic loading. The dimensions of the fatigue specimens are $5 \times 5 \times 56\,\text{mm}^3$, with a gauge section of $5 \times 5 \times 16\,\text{mm}^3$. Symmetrical push–pull cyclic deformation tests were performed at room temperature in air using a Shimadzu servohydraulic testing machine with a constant plastic shear strain amplitude of 1×10^{-3} control. A triangular waveform with a frequency of $0.2\,\text{Hz}$ was used and the test was terminated at $\sim$1500 cycles when the PSBs are well observed and no DBs have been obviously observed for the copper single crystals.

Before and after fatigue tests, the specimens were electropolished to produce a mirror-like surface for microstructure observation. The gauge sections of fatigued copper single crystal samples were sectioned into many pieces with dimensions as mentioned in (1) above and then used for dynamic testing.

(3) The fatigued specimens had dimensions of $5 \times 5 \times 4\,\text{mm}^3$. A steel stopper ring with designed length was placed outside each specimen (see figure 1). During dynamic loading, the deformation process could 'freeze' at different times due to the resistance of the rigid steel stopper rings with different lengths.

Dynamic deformation was conducted on a split-Hopkinson pressure bar apparatus. The strain rates were determined to be in the range $2 - 9 \times 10^3\,\text{s}^{-1}$ for the specimens with different heights. After dynamic deformation, the ASBs were examined in a light microscope and SEM, and the dislocation configurations that developed during fatigue and altered by the dynamic deformation were observed with the ECC technique in an SEM Cambridge S360.
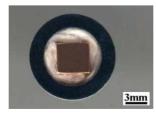

Figure 1. Assembly of a specimen with a steel stopper ring.

3. Results and discussion

3.1. *Before and after cyclic straining: ASB formation under different strain rates*

Before and after cyclic straining, the copper single crystal with loading direction [$\bar{3}$ 4 7], was selected to conduct dynamic deformation under different stain rates.

3.1.1. ASB formation before and after cyclic straining.
The ASB formation in the specimens without cyclic pre-straining can be observed as shown in figure 2. However, the appearance of ASBs was not clear whether the loading rate was higher or lower. This result is consistent with previous findings [28].

   When specimens were subjected to cyclic straining, before dynamic deformation, the dislocation configurations with PSBs and vein structures were well developed as shown in figure 3. In the (15 $\bar{4}$ 9) plane, the PSBs and vein structures can be clearly distinguished (figure 3a). On the top surface (figure 3b, plane ($\bar{4}$ $\bar{8}$ 3)) the vague traces of PSBs can also be seen without much difficulty. The PSBs have the width of 1–2 µm and the spacing of ~10 µm.

   After dynamic deformation, the ASBs can be easily recognized on the sample surfaces. The dislocation structures of ASBs could be detected by the ECC technique, as shown in figure 4.

3.1.2. Width and spacing of ASBs under different strain rates.
The appearances of ASBs in the fatigued copper single crystal at different strain rates are shown in figure 5.

   At strain rates of 2000, 4000 and 8000 s^{-1}, the average widths of ASBs are about 30, 6 and 4 µm, respectively. Correspondingly, the average spacings of ASBs are 230, 40 and 30 µm respectively. The width and spacing of ASBs at different strain rates are shown in figure 6. It is shown that the width and spacing of PSBs clearly depend on the strain rates. The strain rate is higher, while both the width and spacing
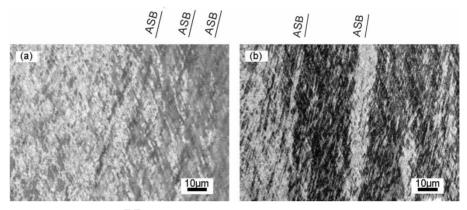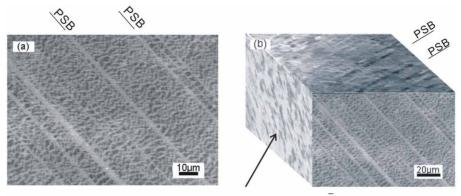

Figure 2.   ASBs in the ($\bar{4}$ $\bar{8}$ 3) plane of the copper single crystal without pre-cyclic straining: (a) strain rate 9000/s, axial strain −67.5%; (b) strain rate 4500/s, axial strain −60.4%.

Figure 3. Persistent slip bands (PSBs) and vein structures of the fatigued copper single crystal: (a) (15 $\bar{4}$ 9) plane, (b) microstructure stereograph of the fatigued copper single crystal.
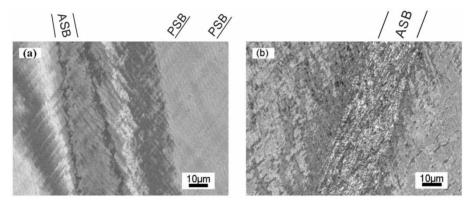

Figure 4. Microstructure in ($\bar{4}$ $\bar{8}$ 3)plane of the fatigued copper single crystal deformed under high strain rate of 4000/s, axial strain (a) −13.4%, (b) −62.6%.

are smaller. However, the volume fractions of ASBs formed under different strain rates are almost constant at 0.14.

Grady and Kipp [34] proposed an approach (called here, the GK model) to determine spatial distribution of shear bands. They used the concept of momentum diffusion. A simple constitutive equation, $\tau = \tau_0[1 - a(T - T_0)]$, was applied; a is a thermal softening parameter; τ_0 and T_0 are reference shear stress and temperature, respectively. Work hardening and strain rate sensitivity are neglected. The predicted ASB spacing, L_{GK}, is:

$$L_{GK} = 2\left(\frac{9kC}{\dot{\gamma}^3 a^2 \tau_0}\right)^{1/4} \qquad (1)$$

where k is the thermal conductivity, C the heat capacity and $\dot{\gamma}$ the strain rate.
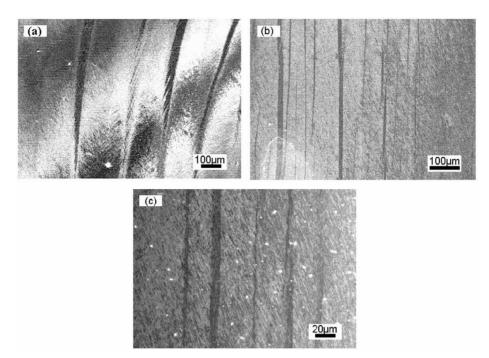
Figure 5. ASBs formed in the fatigued copper single crystal under different strain rates: (a) 2000/s, (b) 4000/s and (c) 8000/s.
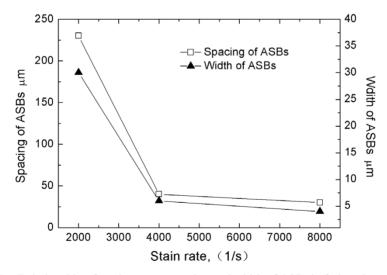

Figure 6. Relationship of strain rate vs. spacing and width of ASBs in fatigued copper single crystals.

Wright and Ockendon [35] developed their theoretical model (WO model), based on the analysis of small perturbations. The constitutive equation for a rate-dependent material was used as $\tau = \tau_0[1 - a(T - T_0)](\dot{\gamma}/\dot{\gamma}_0)^m$, here m is the strain rate sensitivity. The ASB spacing, L_{WO}, is:

$$L_{WO} = 2\pi\left(\frac{kCm^3}{\dot{\gamma}^3 a^2 \tau_0}\right)^{1/4}. \tag{2}$$

Recently, Molinari [36] modified the WO model by considering strain hardening of the materials (M model). The predicted ASB spacing, L_M, is:

$$L_M = \frac{2\pi}{\xi_0}\left(1 + \frac{3\rho C(\partial\dot{\gamma}/\partial\gamma)}{4\beta\tau_0(\partial\dot{\gamma}/\partial T)}\right)^{1/4} \tag{3}$$

where ξ_0 is the wave number, and β is the rate of plastic work transformed into heat. For a constitutive equation concerning linear thermal softening, i.e.:

$$\tau = \mu_0(1 - aT)(\gamma + \gamma_i)^n \dot{\gamma}^m \tag{4}$$

where μ_0 is a constant, γ_i is the pre-strain, and n is the work hardening exponent.

The spacing of ASBs with work hardening effect is obtained as follows:

$$L_M = 2\pi\left(1 - \frac{3\rho Cn(1 - aT)}{4\beta\tau_0 a\gamma}\right)^{-1}\left(\frac{kCm^3(1 - aT_0)^2}{(1 + m)\dot{\gamma}^3 a^2 \tau_0}\right)^{1/4}. \tag{5}$$

The above predictions are classified into two types: momentum diffusion to describe the later stage of shear localization (GK model) and the perturbation analysis to explain the initial growth of ASBs at the early stage (WO and M models). They can also be expressed as [37]:

$$L_{GK} = 2\pi\left(\frac{kC}{\dot{\gamma}^3 a^2 \tau_0}\right)^{1/4} \bullet \frac{9^{1/4}}{\pi} \tag{6}$$

$$L_{WO} = 2\pi\left(\frac{kC}{\dot{\gamma}^3 a^2 \tau_0}\right)^{1/4} \bullet m^{3/4} \tag{7}$$

$$L_M = 2\pi\left(\frac{kC}{\dot{\gamma}^3 a^2 \tau_0}\right)^{1/4} \bullet \left(\frac{m^3(1 - aT_0)^2}{(1 + m)}\right)^{1/4} \tag{8}$$

For $n = 0$ and $\beta \approx 1$.

For coarse-grained pure copper polycrystals, the strain rate sensitivity, m, is about 0.011 [38] and for nanocrystalline pure coppers is about 0.036 [39], so that we may expect that the m value is still small for copper single crystals and a rough estimation of $m \approx 0.01$ could be acceptable.

For pure copper, $k = 398$ W/m K and $C_p = 385$ J/kg K [40] and $\tau_0 = 220$ MPa [41]. The thermal softening factor, a, has not been reported in the literature, however, for copper a value of about 1 for w was reported in the thermal softening term,

$(1 - ((T - T_r)/(T_m - T_r))^w)$, in the Johnson–Cook equation [42, 25]. If $T_m = 1356\,K$ and $T_r = 298\,K$, the thermal softening factor, a, can be roughly estimated as $9.5 \times 10^{-4}/K$. This value is rather close to the softening factors of $1.0 \times 10^{-3}/K$ for Ti and Ti alloys [37]. From above values, the ASB spacing can be estimated by equations (6), (7) and (8) as listed in table 1.

From table 1, one can see that the predicted ASB spacing by the GK model is about one-order of magnitude larger than that predicated by the WO or M models. Wright and Ockendon [35] have pointed out that the perturbation analysis in their paper is based on a linearization about the state of uniform, steady shearing; it applies to the early stages of localization only. Therefore, a smaller ASB spacing can be expected for the WO and M models. Xue *et al.* [37] have verified that the ASB spacing predicted by the WO and M models for pure titanium is consistent with the experimental results. However, in the present paper, the predicted ASB spacings by the WO and M models are still one-order of magnitude larger than those observed experimentally for fatigued samples. Possible reasons why the predicted values are inconsistent with the experimental results are as follows.

Firstly, the models referred to are based on linear perturbation analysis of the fundamental mechanical equations. Their predictions are accurate for the case in which the liner and nonlinear effects are similar. In the present study, the prediction of ASB spacing for fatigued copper single crystals may be rather poor due to severe heterogeneities induced by cyclic pre-straining. Mayers *et al.* [26] pointed out that microstructural heterogeneities rather than strain/temperature perturbations or momentum diffusion are possibly the determining factors in spacing. In the present work, the dislocation configurations were well developed in the single crystals during fatigue; especially the PSBs with about 1 μm width and 10 μm spacing were rather uniformly distributed in the sample. When a dynamic loading is applied, the abundant interfaces between the PSBs and the matrix could be the preferential sites for ASB formation and, in turn, might result in the smaller ASB spacing.

Secondly, the models mentioned above are based on the fact that thermal softening is the key factor for ASB formation in dynamic deformation and geometric softening is neglected. This is good enough for modelling ASB formation in polycrystals deformed under very high strain rates. However, geometric softening caused by crystallographic rotation during deformation can frequently occur in metal-forming; for example, in conventional rolling process, the mechanism of shear band formation can be attributed to geometric softening [29], and the thermal softening can be neglected. In the present experiment, the shear band formation in copper single crystals induced by dynamic deformation could be attributed to both

Table 1. Predicted and observed ASB spacing.

Strain rate 1/s	ASB spacing mm			
	Experiment	G–K	W–O	M
2000	0.23	59.2	3.33	2.90
4000	0.04	35.4	1.99	1.74
8000	0.03	21.1	1.19	1.03

thermal softening and geometric softening. In other words, during deformation process, the orientation of the single crystal will vary and some favourable slip systems may come into operation. This will stimulate easier ASB formation and, in turn, may result in a smaller ASB spacing.

The effects of orientations of crystals on ASB formation, particularly on the critical strain, is discussed below.

3.2. *ASB formation for single crystals with different orientations*

The axial orientations of four copper single crystals investigated are shown in the standard stereographic triangle (figure 7). In the figure, the initial axial orientations of [$\bar{1}$ 2 4], [$\bar{3}$ 4 7], [$\bar{4}$ 15 16] and [$\bar{1}$ 8 11] are indicated by A, B, C and D, respectively, for the four copper single crystals. Since fatigued specimens form ASBs rather more easily, the cyclic pre-straining was conducted for each single crystal. The loading directions both in cyclic straining and dynamic loading are identical for each single crystal. In dynamic testing, only the strain rate of $4000\,s^{-1}$ was applied. As mentioned in section 2, the steel stopper rings with different lengths were used in dynamic testing to determine the critical strain for ASB formation. During dynamic deformation, the axial orientation will vary. In figure 7, corresponding initial orientations of single crystals of A, B, C and D, the A′, B′, C′ and D′ are, respectively, the orientations where the ASB formation was observed after dynamic testing.
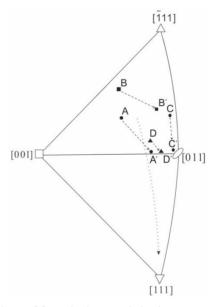

Figure 7. Axial orientations of four single crystals in the stereographic triangle. A, B, C, D are initial orientations, and A′, B′, C′ and D′ are the orientations where the ASB formation was observed.

Table 2. Geometric relations among ASB plane, loading axis and some special planes.

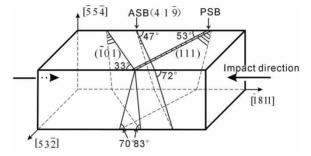| Single crystal	Loading axis	Plane of ASB	Angles between ASB plane and			Critical Strain I%	Critical Strain II%
			Loading axis	DBI habit plane $(1\,1\,1)$	DBII habit plane $(\bar{1}\,0\,1)$		
SC-A	$[\bar{1}\,2\,4]$	$(3\,6\,7)$	56°	17°	73°	−18.5	−17.5
SC-B	$[\bar{3}\,4\,7]$	$(56\,3\,\overline{73})$	58°	85°	8°	−10.8	−12.5
SC-C	$[\bar{4}\,15\,16]$	$(\bar{7}\,5\,5)$	57°	79°	31°	−22.7	−16
SC-D	$[\bar{1}\,8\,11]$	$(4\,1\,\bar{9})$	45°	76°	21°	−16.7	−12

Figure 8. Illustration of geometric relations among ASB plane, primary slip plane (same as PSB plane) and DBII plane of single crystal $[\bar{1}\,8\,11]$.

3.2.1. The critical strain for ASB formation and the orientation of ASB plane.
In each single crystal, four to six samples with different lengths of steel stopper rings were used for dynamic testing to determine the critical strain. The critical strains for ASB formation were determined by observing whether the ASBs appeared on the sample surface or not, as listed in table 2, in which they are named as critical strain I. The critical strains may also be determined from dynamic stress–strain curves, and named as critical strain II. In the next section, we will address how to determine these values by dynamic stress–strain curves.

The orientation of an ASB plane can be determined based on the traces appearing on the sample surfaces. For example, $[\bar{1}\,8\,11]$ single crystal, the geometric relations of an ASB with loading axis, primary slip plane (same as the PSB plane) and other elements are shown schematically in figure 8. The plane of the ASBs can be found close to $(4\,1\,\bar{9})$. It should be noted that the ASB plane is not a habit plane, since various orientations of the ASBs can be formed for different single crystals as listed in table 2. Also, the ASB plane is not strictly a crystallographic plane due to the complexity of the ASB formation. Here, we use a crystallographic plane index to denote it for convenience.

Considering the errors of critical strains obtained by examining post-deformation specimens and dynamic stress–strain curves, it is better to use the average values for further discussion. From table 2, the average values of critical strain I and critical

strain II for single crystals A, B, C and D are −18, −11.7, −19.4 and −14.4%, respectively. It clearly shows that the critical strains for single crystals are orientation-dependent. The critical strains are lower for B and D single crystals and greater for A and C single crystals. Hereafter, the single crystals A, B, C and D are named as SC-A, SC-B, SC-C and SC-D, respectively, for simplicity.

From table 2, one can see that the orientations of the ASB planes also depend on the axial orientations (loading directions) of single crystals. The angles between loading axis and the ASB planes are in the range 45–60°. For SC-B, the angle between the ASB plane and the habit plane of DBII is the smallest; however, for SC-A it is the largest.

3.2.2. A micro-mechanism for ASBs formation.

The initial orientations of four single crystals are all single-slip oriented as shown in figure 7. SC-A is a typical single-slip oriented and after fatigue the dislocation patterns are two-phase structures, i.e. PSB ladders embedded in matrix veins [6–8], as shown in figure 3. SC-B is close to the [001]–[$\bar{1}$11] duplex slip side of the stereographic triangle, particularly close to [$\bar{1}$22]. The dislocation patterns of single crystal [$\bar{1}$22] are also PSB ladders and veins, as pointed out by Li *et al.* [43]. SC-C is close to the [011]–[$\bar{1}$11] duplex slip side, particularly close to [$\bar{2}$55]. The dislocation patterns of single crystal [$\bar{2}$55] are PSB ladder-like and cell structures [43]. SC-D is rather close to the [001]–[011] duplex slip side, particularly close to [034]. The dislocation patterns of single crystal [034] are PSB ladders embedded in veins, cells and occasionally labyrinth structures [44]. In the present experiments, however, the common feature of microstructures of the four fatigued single crystals is that the PSB ladders are embedded in matrix veins or cells.

Over the stain rate range $(2 - 9 \times 10^3 \, \mathrm{s}^{-1})$ applied in the present dynamic testing, the dominant micro-deformation mechanism is dislocation motion. After dynamic loading, the appearances of ASBs can be seen as in figures 4, 5 and 9a. After close examination of the sample surface, the primary slip operation along PSBs can be confirmed; for example, in figure 4a, the primary slip traces along PSBs can be seen without much difficulty. In this figure, the secondary slip and multi-slip can also be seen near the ASB. A just initiated ASB is shown in figure 9b in which the shearing of ASB results in the deviation of PSBs from their original directions by about 10°. The typical microstructure of the ASBs is elongated cell structure (figure 9c) at the initiation stage. As the deformation continues and as the misorientation increases, these cells become elongated subgrains (figure 9d), which are quite similar to those found in copper polycrystals [45].

Reid [46] pointed out that, in a unidirectional compressive test of an fcc single crystal, on the [001]–[$\bar{1}$11] side of stereographic triangle, the duplex slip is critical, which means it is unstable to small fluctuation of the loading axis, and single slip may subsequently predominate. In other words, once one of the two equivalent slip systems operates, it will keep operating. On the [001]–[011] side, the duplex slip is conjugate, which means it should be stable to fluctuation of orientation. In other words, the two equivalent slip systems will operate alternatively. On the [011]–[$\bar{1}$11] side, the duplex slip is coplanar, which means that the two equivalent slip systems share the same slip plane. Reid [46] also pointed out that in a unidirectional
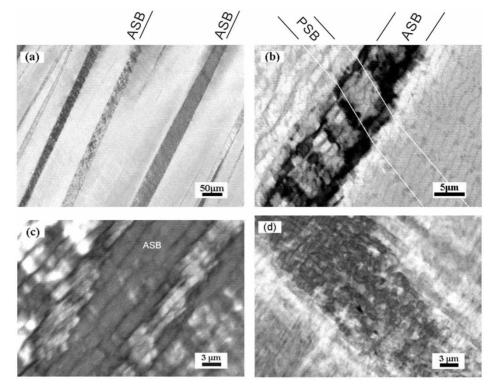
Figure 9. Appearances and microstructures observed by SEM–ECC technique: (a) ASBs in SC-B, (b) shearing of an ASB results in the PSBs deviating from their original direction by about 10° in SC-B, (c) ASB microstructure in SC-C, (d) ASB microstructure in SC-D.

compressive test, the loading axis of an fcc single crystal rotates in such a way that it approaches the normal to the primary slip plane (111). In the present dynamic compressive deformation, the loading axes of the four crystals were basically rotated toward [111], as shown in figure 7, which is in agreement with the Reid's argument. When the ASBs appeared, the loading axes of all single crystals, except SC-B, rotated towards and almost reached the [001]–[011] side where the conjugate slip operated. Also, the loading axis of SC-B basically rotated towards the [001]–[011] side; however, it needs much larger strain to reach this side since the initial loading axis of SC-B is far away from the side. In fact, the loading axis of SC-B rotated to the place where it is rather close to the coplanar duplex slip [011]–[$\bar{1}$11] side, it may lead to much complex slip.

Figure 10 shows the dynamic engineering stress–strain curves. For a typical single-slip oriented SC-A, the first stress plateau indicates the primary slip operation, the second indicates the secondary slip operation and the third indicates ASB formation. The critical strain might be determined as −17.5% for SC-A (figure 10a). Similarly, the critical strains could be determined as −16 and −12% for SC-C (figure 10c) and SC-D (figure 10d), respectively. When the loading axes of the above three single crystals rotated to the [001]–[011] side closely, the conjugate
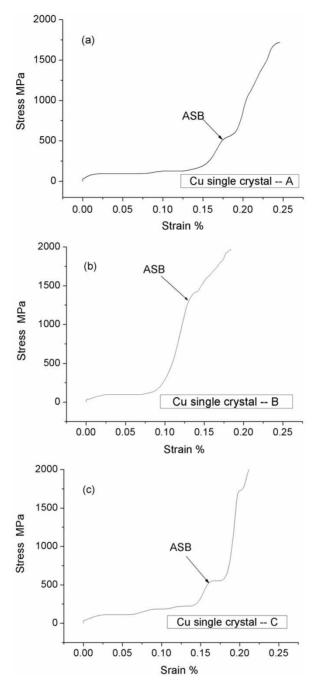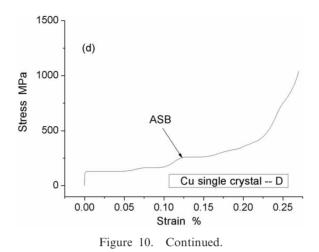
Figure 10.   Stress–strain curves of the fatigued copper single crystals with different orientations under strain rate of 4000 1/s. (a) SC-A, (b) SC-B, (c) SC-C, (d) SC-D.

Figure 10. Continued.

duplex slip operated. At the early stage of the secondary slip, the second stress plateau occurred due to the stable fluctuation of orientation, as mentioned above. After that, the multi-slip will be dominant due to increase in dislocation density and it leads to a drastic increase in stress. For SC-B, the first stress plateau, indicating primary slip, can also be clearly observed; however, no stress plateau indicated the secondary slip operation could be clearly observed. This is because the initial loading axis of SC-B is close to the critical duplex slip $[001]$–$[\bar{1}11]$ side; once the deformation starts, the single slip may subsequently predominate [46]. When the loading axis is rotated to the coplanar duplex slip side where two equivalent slip systems share the same slip plane, as soon as the secondary slip operates, the multi-slip could be predominant due to the complex interactions among the dense dislocations in the same slip plane. From the stress plateau of ASB formation, the critical strain might be found as -12.5% (figure 10b).

   In compressive deformation, the loading axes of four crystals should rotate along the large circles toward $[111]$ and should meet the $[001]$–$[011]$ side at some point. Critical strains versus the angles between the initial loading axis and the point intersected at the $[001]$–$[011]$ side are shown in figure 11a. Note that the loading axes oriented close to the conjugate duplex slip side ($[001]$–$[011]$) need lower critical strains for ASB formation (e.g. SC-D); those close to the critical duplex slip side ($[001]$–$[\bar{1}11]$) also need lower critical strain (e.g. SC-B). By contrast, those loading axes oriented close to the coplanar duplex slip side ($[011]$–$[\bar{1}11]$) (e.g. SC-C) and the loading axes located in a typical single-slip oriented region (e.g. SC-A) need greater critical strains for ASB formation.

   Critical strains versus angles between ASB plane and DBII habit plane ($\bar{1}\,0\,1$) are shown in figure 11b. Generally speaking, the smaller the angle, the lower the critical strain will be. This means that an ASB is easier to form along DBII. For SC-A, the angle is the largest and the critical strain should be greatest. The reasons why the critical strain is smaller than expected is found in table 2, in which the angle between the ASB plane and DBI habit plane (111) is the smallest for SC-A. This means that an ASB is also easier to form along DBI. The critical strain for SC-C is
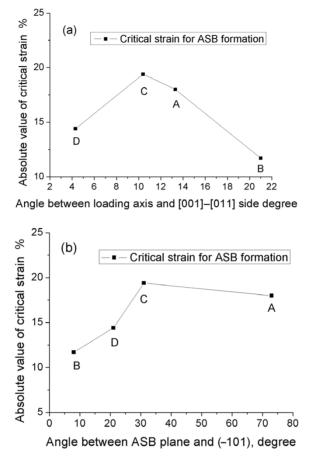
Figure 11.   In four fatigued single crystals, the critical strains vs. (a) the angles between initial loading axis and point intersected at [001]–[011] side, (b) the angles between ASB plane and DBII habit plane ($\bar{1}\,0\,1$).

the greatest (figure 11), and the angle between the ASB plane and DBII plane, as well as the angle between the ASB plane and DBI plane, are both larger (table 2).

From these observations, a micro-mechanism for ASB formation in fatigued copper single crystals could be proposed as follows:

(1) When impact loading was applied (figure 12a), the dislocations in the PSBs were the first to operate since the PSBs are soft [10] and located in the primary slip plane (figure 12b). In the PSBs, the screw dislocations move with less resistance [8], which leads to the first stress plateau occurring in the dynamic stress–strain curves.

(2) As the deformation continues, the loading axis rotates towards the duplex slip side, the secondary slip will preferentially operate near heterogeneities, particularly near the interface between the PSBs and the matrix (figure 12c). This may result in the emergence of the second stress plateau.
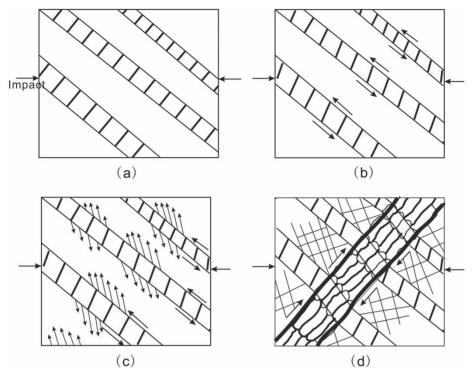
Figure 12. Schematic of ASB formation in a fatigued copper single crystal.

(3) With increasing dislocation density, the multi-slip operates and the stress to overcome dislocation barriers increases drastically. However, once the dislocations assisted by the stress wave break through the network in a suitable direction, an ASB forms (figure 12d). At this moment, thermal softening could play an important role in ASB formation due to large plastic work released in a short time interval.

The above scheme works particularly well for the typical single-slip oriented SC-A; however, for other single crystals orientated close to different duplex slip sides in the stereographic triangle, the ASB formation process could be slightly different due to their specific orientations. For example, in SC-D, after primary and secondary slip, ASB formation may occur before the occurrence of multi-slip. In SC-C, ASB and multi-slip seem to occur concomitantly. In SC-B, secondary slip and multi-slip operate simultaneously.

4. Conclusions

From the experimental results and discussion, some conclusions may be drawn:

- Under dynamically compressive deformation, the spacing of ASBs in fatigued copper single crystals is about one-order smaller than that predicted by

theoretical models. For ASB formation, those models involving the thermal softening, geometric softening, as well as heterogeneities in the material, are essential.

- The critical strains for ASB formation in fatigued copper single crystals are orientation-dependent. Under dynamically compressive deformation, the critical strain is smaller if the loading axis is close to the critical or conjugate duplex slip side in the standard stereographic triangle, and the critical strain is greater if the loading axis locates in the typical single-slip oriented region or close to the coplanar duplex slip side.

Acknowledgements

References

[1] N. Thompson, N.J. Wadsworth and N. Louat, Phil. Mag. **1** 113 (1956).
[2] E.E. Laufer and W.N. Robert, Phil. Mag. **14** 67 (1966).
[3] P. Lukas, M. Klesnil and J. Krejci, Phys. Status Solidi. **27** 545 (1968).
[4] D.F. Watt, J.D. Embury and R.K. Ham, Phil. Mag. **17** 199 (1968).
[5] P.J. Woods, Phil. Mag. **28** 155 (1973).
[6] S.J. Basinski, Z.S. Basinski and A. Howie, Phil. Mag. **19** 899 (1969).
[7] J.G. Antonopoulos, L.M. Brown and A.T. Winter, Phil. Mag. **34** 549 (1976).
[8] H. Mughrabi, F. Ackermann and K. Herz, in *STP675* (ASTM, Philadelphia, 1979), p. 69.
[9] D. Kuhlmann-Wilsdorf and C. Laird, Mater. Sci. Eng. **27** 137 (1977).
[10] A.T. Winter, Phil. Mag. A **37** 457 (1978).
[11] T. Tabata, H. Fujita, M. Hiraoka, *et al.*, Phil. Mag. A **47** 841 (1983).
[12] F. Ackermann, L.P. Kubin, J. Lepinoux, *et al.*, Acta Metall. **32** 715 (1984).
[13] N.Y. Jin, Acta Metall. **37** 2055 (1989).
[14] U. Holzwarth and U. Essmann, Appl. Phys. A **57** 131 (1993).
[15] O.B. Pedersen, Phil. Mag. A **73** 829 (1996).
[16] Z.R. Wang, Scripta Mater. **39** 493 (1998).
[17] S.X. Li, Y. Li, G.Y. Li, *et al.*, Phil. Mag. A **82** 867 (2002).
[18] S.X. Li, M.Y. Li, R. Zhu, *et al.*, Phil. Mag. **84** 3323 (2004).
[19] X.W. Li, Z.G. Wang and S.X. Li, Phil. Mag. A **80** 1901 (2000).
[20] S.X. Li, X.W. Li, Z.F. Zhang, *et al.*, Phil. Mag. A **82** 3129 (2002).
[21] C. Zener and J.H. Hollomon, J. App. Phys. **15** 22 (1944).
[22] Y.L. Bai, J. Mech. Phys. Solids **30** 195 (1982).
[23] T.W. Wright and R.C. Batra, Int. J. Plast. **1** 205 (1985).
[24] A. Molinari and R.J. Clifton, Trans. ASME **54** 806 (1987).
[25] M.A. Meyers, U. Andrade and A.H. Chokshi, Metall. Mater. Trans. A **26** 288 (1995).
[26] M.A. Meyers, V.F. Nesterenko, J.C. LaSalvia, *et al.*, Mater. Sci. Eng. A **317** 204 (2001).
[27] Y.W. Chang and J.R. Asaro, Acta Metall. **29** 24 (1981).
[28] M.M. Rashid, G.T. Gray and S. Nemat-Nasser, Phil. Mag. A **65** 707 (1992).

[29] I.L. Dillamore, J.G. Roberts and A.C. Bush, Metal. Sci. **13** 73 (1979).

[30] G.Q. Cheng and S.X. Li, Mater. Sci. Technol. **21** 813 (2005).

[31] R. Zauter, F. Petry, M. Bayerlein, *et al.*, Phil. Mag. A **66** 425 (1992).

[32] A. Schwab, J. Bretschneider, C. Buque, *et al.*, Phil. Mag. Lett. **74** 449 (1996).

[33] J. Ahmed, A.J. Wilkinson and S.G. Roberts, Phil. Mag. Lett. **76** 237 (1997).

[34] D.E. Grady and M.E. Kipp, J. Mech. Phys. Solids **35** 95 (1987).

[35] T.W. Wright and H. Ockendon, Int. J. Plast. **12** 927 (1996).

[36] A. Molinari, J. Mech. Phys. Solids **45** 1551 (1997).

[37] Q. Xue, M.A. Meyers and V.F. Nesterenko, Acta Mater. **50** 575 (2002).

[38] P.I. Polikin, G.Y. Gun and A.M. Galkin, in *Handbook of Resistance to Plastic Deformation of Meals and Alloys* (Metallurgy Press, Moscow, 1976), p. 339.

[39] L. Lu, S.X. Li and K. Lu, Scripta Mater. **45** 1163 (2001).

[40] M.A. Shehadeh, H.M. Zbib and T.D.D.L. Rubia, Phil. Mag. **85** 1667 (2005).

[41] S. Nemat-Nasser and Y.L. Li, Acta Mater. **46** 565 (1998).

[42] G.R. Johnson and W.H. Cook, in *Proceedings of the 7th International Ballistics Symposium*, The Hague (1983), p. 541.

[43] X.W. Li, Z.F. Zhang, Z.G. Wang, *et al.*, Defects Diffus. Forum **188/190** 153 (2001).

[44] B. Gong, Z.R. Wang, Z.G. Wang, *et al.*, Mater. Sci. Eng. A **210** 94 (1996).

[45] U.R. Andrade, M.A. Meyers, K.S. Vecchio, *et al.*, Acta Metall. Mater. **42** 3183 (1994).

[46] C.N. Reid, *Deformation Geometry for Materials Scientists* (Pergamon Press, Oxford, 1973).